

Achievable Precision for Optical Ranging Systems

Bruce Moision and Baris I. Erkmen

Jet Propulsion Laboratory, California Institute of Technology,
4800 Oak Grove Dr., Pasadena, CA 91109

ABSTRACT

Achievable RMS errors in estimating the phase, frequency, and intensity of a direct-detected intensity-modulated optical pulse train are presented. For each parameter, the Cramèr-Rao-Bound (CRB) is derived and the performance of the Maximum Likelihood estimator is illustrated. Approximations to the CRBs are provided, enabling an intuitive understanding of estimator behavior as a function of the signaling parameters. The results are compared to achievable RMS errors in estimating the same parameters from a sinusoidal waveform in additive white Gaussian noise. This establishes a framework for a performance comparison of radio frequency (RF) and optical science. Comparisons are made using parameters for state-of-the-art deep-space RF and optical links. Degradations to the achievable errors due to clock phase noise and detector jitter are illustrated.

Keywords: optical science, estimation theory, quantum-limited sensing, photon-counting detectors, Cramèr Rao bounds

1. INTRODUCTION

In this paper we make a preliminary study of the potential for science derived from deep-space optical communication links. Optical links in development at the Jet Propulsion Laboratory utilize intensity-modulation, noncoherent photon-counting receivers, and carriers in the infrared regime, from 1.0 to 1.5 μm .¹ These choices are made to maximize the power efficiency of the link and take into account constraints of current technology. In this paper, we consider deriving science measurements from this optical telemetry link. Throughout we use the shorthand ‘optical’ to refer to an intensity-modulated infrared signal received with a noncoherent photon-counting receiver. We would like to determine what science one can derive from observing the telemetry link. We may separate this into two sub-problems:

1. How accurately can we measure distortions of an intensity-modulated optical signal?
2. What science can be performed given the accuracy of the measurements?

In this paper we address the first question, and determining the accuracy with which one may measure phase, frequency, and intensity of an optical signal. We compare this to the conventional state-of-the-art estimation from coherently demodulated microwave, or radio-frequency (RF), carriers. Conventional RF science is derived from a ranging clock, which may be modeled as a sinusoid received in AWGN, see, e.g., [2, Chapter 3],

$$y(t) = A \cos(2\pi f_r t - \phi) + n(t) \quad (1)$$

where A is the signal amplitude, f_r is the range clock frequency, ϕ is the phase, and $n(t)$ is additive white Gaussian noise. An example is illustrated in Figure 1 for $f_r = 1$ MHz. Estimating the instantaneous phase, frequency, and amplitude of the RF waveform allows one to determine properties of processes that distort these parameters. For example, spacecraft range may be determined from the transmitter delay, via an estimate of the phase, and velocity determined by the induced doppler shift, via an estimate of the frequency. Analogous properties of the

©California Institute of Technology. Government sponsorship acknowledged. Send correspondence to bmoision@jpl.nasa.gov. The research described in this publication was supported by the DARPA InPho program under contract PROP.81-17433, and the JPL R&TD Program, and was carried out by the Jet Propulsion Laboratory, California Institute of Technology, under a contract with the National Aeronautics and Space Administration

signal waveform may be extracted from the photocurrent generated from an intensity-modulated optical signal incident on a photon-counting detector. The photocurrent, when normalized by the electron charge, is modeled as a random Poisson point process, governed by a rate function

$$l(t) = l_p \int_{kT_r - \infty}^{\infty} \rho(t - kT_r - \phi') + l_b \quad (2)$$

where l_p denotes the peak photo-electron rate in pe/sec, $\rho(t)$ is the intensity pulse shape, satisfying $1 \geq \rho(t) \approx 0$, T_r is the repetition period, ϕ' is the phase, and l_b is the mean photo-electron rate from other sources, such as thermal* and dark noise †. Figure 2 illustrates an example rate function and a realization of a random point process, representing photo-electron arrivals, induced by it. Analogous to the parameter estimates obtained from an RF carrier, we may estimate l_p , T_r , and ϕ , based on observing photo-electron emissions governed by the rate function $l(t)$.

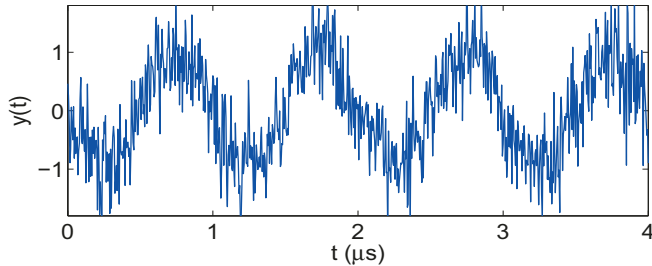


Figure 1. Coherent Microwave (RF) Received Signal

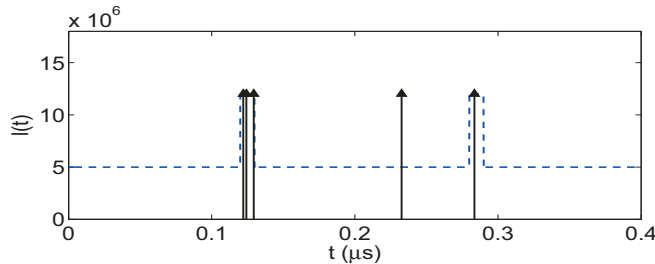


Figure 2. Noncoherent Infrared (Optical) Received Signal

The paper is organized as follows. In Section 2, we establish a model and general framework for studying the problem, and derive Cramer-Rao-bounds (CRBs) and maximum-likelihood (ML) estimators. In Section 3 we review the analogous results for the RF signal and draw comparisons utilizing parameters for current state-of-the-art links. In Section 4 we examine degradations to the ideal performance due to detector and clock jitter, and in Section 5 we briefly discuss the results.

2. PARAMETER ESTIMATION FOR A DIRECT-DETECTED OPTICAL SIGNAL

In any implementation of a parameter estimation system, many errors contribute to the overall performance, such as clock drift, clock offset, transmitter jitter and detector jitter. In this section we consider the performance of an ideal system, limited only by the received signal and noise powers and observation times. In Section 4 we introduce degradation due to detector jitter and clock phase noise. Thus, the performance reported herein is a lower bound on the performance of practical systems.

*We assume thermal noise is multi-mode with sufficient number of modes to justify a Poisson approximation

†Although dark noise does not, strictly speaking, generate photo-electrons, for convenience we utilize units of photo-electrons for all electrons.

2.1 Channel Model

We model the received signal as follows. A periodic repeating optical pulse train is transmitted in vacuum. At the receiver, the light is focused on an ideal photodetector. The ideal detector has negligible thermal noise, and sufficient bandwidth that individual photon arrival times may be observed at its output. The output is a random photocurrent, which, normalized by the electron charge, is accurately modeled as an inhomogeneous Poisson process with rate function given by (2).

The signal parameters are determined by the underlying communications link, which we presume is implemented with pulse-position-modulation (PPM), wherein time is divided into slots of duration T_s , with T_s on the order of the pulse width. It is convenient, in this context, to normalize time to be in units of slots, that is, defining

$$u \stackrel{\text{def}}{=} t/T_s, \quad (3)$$

the rate function of the inhomogeneous Poisson process that describes the photocurrent is expressed as

$$\Lambda(u) \stackrel{\text{def}}{=} T_s l(uT_s) = n_s \int_{kT - \infty}^{\infty} g(u - kT - \phi) + n_b, \quad (4)$$

where $n_s \stackrel{\text{def}}{=} l_p \int g(t) dt$ is the mean signal photo-electrons per pulse, $n_b \stackrel{\text{def}}{=} l_b T_s$ is the mean number of noise photo-electrons per slot, $T \stackrel{\text{def}}{=} T_r/T_s$ is the repetition period in slots, $\phi = \phi'/T_s$ is the phase of the periodic waveform, and

$$g(u) = \frac{f(uT_s)}{\int f(uT_s) du} \quad (5)$$

is the normalized pulse shape. We assume a generalized Gaussian pulse,

$$g(u) = \frac{p}{2a\Gamma(1/p)} \exp(-|u/a|^p), \quad (6)$$

where $\Gamma(\cdot)$ is the Gamma function, a is the $1/e$ width of the pulse, and p is the decay rate of the pulse tails. Figure 3 illustrates the pulse for a range of values of p . This parameterized pulse shape models a wide range of practical pulse shapes, from Gaussian ($p = 2$), to square (large p , e.g., $p = 10$ or greater).

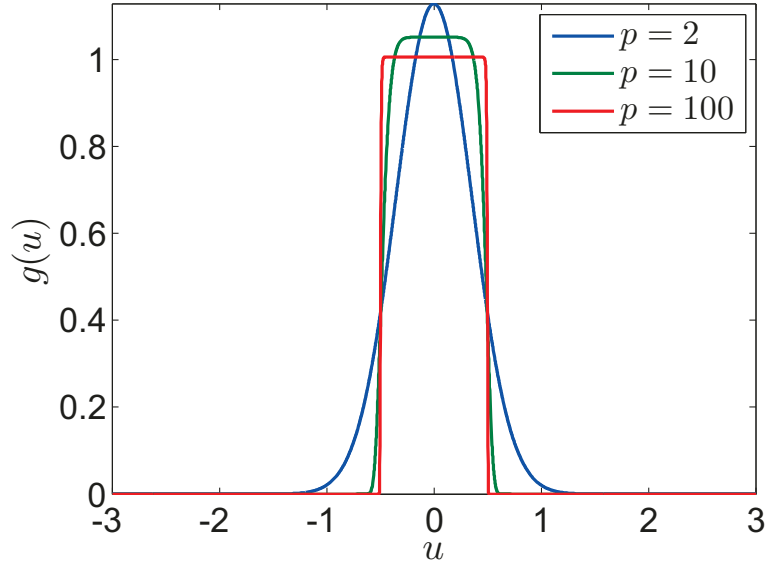


Figure 3. Generalized Gaussian pulse shapes for several decay rates p .

We treat the problems of estimating n_s, T and ϕ . We assume throughout that the unknown parameters are constant over the observation period. We also assume that the noise mean n_b is known[‡]. Estimates are based on the observation of photon arrivals over an interval of duration $T_i = KT$. Suppose that we observe N arrivals at times $\{u_1, u_2, \dots, u_N\}$. The conditional log joint density of the collection of observations is³

$$\log p(\{u_i\}, N) = \begin{cases} \int_{T_i} \Lambda(u) du + \int_{i=0}^{N-1} \log \Lambda(u_i) & , \text{for } N > 0 \\ \int_{T_i} \Lambda(u) du & , \text{for } N = 0. \end{cases} \quad (7)$$

We assume a single parameter is unknown, and all other parameters are known. Let $\theta \in \mathcal{N}(\phi, T, n_s)$ be the unknown parameter. In the following sections we find the maximum-likelihood estimate

$$\hat{\theta}_{\text{ML}} = \arg \max_{\theta} \log p(\{u_i\}, N; \theta) \quad (8)$$

and the CRB, which we show in Appendix A may be expressed as

$$\text{CRB}_{\theta} = \int_{T_i} \sqrt{\frac{(d\Lambda(u)/d\theta)^2}{\Lambda(u)}} du \left[^{-1} \quad (9)$$

which, substituting the rate function (4), yields

$$\text{CRB}_{\theta} = \int_{T_i} \sqrt{\frac{n_s^2 \int_k (\partial g(u - kT - \phi)/\partial \theta)^2}{n_s \int_k g(u - kT - \phi) + n_b}} du \left[^{-1} \quad (10)$$

The mean-squared-error of the ML estimator, $\text{MSE} = E[(\theta - \hat{\theta}_{\text{ML}})^2]$, asymptotically approaches the CRB⁴ in T_i , hence the CRB provides a useful approximation to the performance of the estimator in the limit of long observation times. In the following sections we provide expressions for (8),(10) for each parameter. Throughout we assume the pulses are non-overlapping—a good approximation for $T \in a$, which is typically the case.

2.2 Phase

The ML phase estimate is given by

$$\hat{\phi}_{\text{ML}} = \arg \max_{\phi} \int_{j=0}^{N-1} \log \left(n_s g [u_i - \phi]_T (+ n_b) \right) \quad (11)$$

where $[u]_T \stackrel{\text{def}}{=} (u + T/2 \bmod T) - T/2$. In this expression, from periodicity of the pulse train, arrivals need only be known modulo the period. Note that the ML estimator based on observing K periods of the inhomogenous Poisson process with rate $\Lambda(u)$ is *statistically equivalent* to that based on observing one period of an inhomogenous Poisson process with rate $K\Lambda(u)$.

The CRB is given by⁵

$$\text{CRB}_{\phi} = \int_{-T/2}^{T/2} K \sqrt{\frac{(n_s p u^{p-1} g(u))^2}{a^{2p} (n_b + n_s g(u))}} du \left[^{-1} \quad (12)$$

which may be evaluated numerically. In the asymptotic regions we have

$$\text{CRB}_{\phi} \ll \begin{cases} \frac{1}{Kn_s} \frac{a^2}{p} & , n_s g(0) \in n_b \\ \frac{n_b}{Kn_s^2} \frac{a^2 2^{2-1/p}}{p} & , n_s g(0) \gg n_b. \end{cases} \quad (13)$$

[‡]The noise mean is typically slowly time varying, and may be estimated with an accuracy justifying this assumption.

In our current cases of interest, the signal powers demanded by the communications link put us in the $n_s g(0) \in n_b$ regime, which we'll refer to as the *high SNR* regime. Suppose the time-of-flight of the path is known a-priori to within one period of the pulse train (the period may be increased by transmitting a pseudo-random sequence of pulses to make this assumption valid). Then the phase may be mapped to an estimate of the time-of-flight, and to an estimate of the range. If the transmission path is vacuum, the resulting RMS range error (RMS = $\sqrt{\text{MSE}}$) is

$$\text{RMS}_{\text{range}} \ll \frac{1}{T_i P_r} \frac{hc (aT_s)^2 c^2}{\lambda p} \quad (m)$$

where h is Planck's constant, λ is the carrier wavelength, c is the speed of light in a vacuum, and we've mapped the mean signal photons per pulse to the received power, P_r , as

$$P_r = \frac{n_s hc}{T T_s \lambda} \quad (14)$$

We see that the RMS error is inversely proportional to the square root of the received signal energy, linear in the pulse width (aT_s), and decreases for pulses that are more square (larger p).

2.3 Intensity

The ML estimate of the intensity, $\hat{n}_{s,\text{ML}}$, satisfies

$$\int_{j=0}^{N-1} \frac{g(u_i)}{\hat{n}_{s,\text{ML}} g(u_i) + n_b} \ll K$$

If we approximate the pulse as uniform on $[-\beta, \beta]$ and zero otherwise, we have the approximation

$$\hat{n}_{s,\text{ML}} \ll \frac{1}{K} N_{[-\beta, \beta]} \quad 2\beta n_b \quad (15)$$

where $N_{[t_1, t_2]}$ is the number of arrivals on $[t_1, t_2]$. Estimate (15) is the number of arrivals over an approximate pulse duration, minus the mean noise arrivals on the same period. The CRB is given by

$$\text{CRB}_{n_s} = \left(K \int_{-T/2}^{T/2} \frac{g^2(u)}{n_s g(u) + n_b} du \right)^{-1}$$

which may be evaluated numerically. In the asymptotic regions, we have

$$\text{CRB}_{n_s} \ll \begin{cases} n_s / K & , n_s g(0) \in n_b \\ (n_b / K) \Gamma(1/p) 2^{1/p} / p & , n_s g(0) \gg n_b \end{cases}$$

To make a common comparison later with the RF case, we convert the estimate of n_s to an estimate of the received power via (14), with high SNR CRB

$$\text{CRB}_{P_r} \ll \frac{P_r hc}{T_i \lambda}$$

In practice, we may be more interested in changes to the power, rather than the absolute power, and, hence, the fractional error

$$\frac{\text{RMS}_{P_r}}{P_r} \ll \left(\frac{1}{P_r T_i} \left[\right] \right) \frac{hc}{\lambda} \left[\right]$$

2.4 Period

For the baseband photocurrent process, it is more natural to derive the frequency estimate from an estimate of the period T . Let the known phase be zero: $\phi = 0$. Recall that $T_i = KT$. Let $\tilde{K} = \lfloor KT/\tilde{T} \rfloor$, the number of pulses that would occur in the interval T_i under the hypothesis $T = \tilde{T}$. The ML estimate may be written as

$$T_{\text{ML}} = \arg \max_{\tilde{T}} J(\tilde{T})$$

$$J(\tilde{T}) = n_s \int_{u=0}^{\tilde{K}-1} \int_0^{k\tilde{T}} \sqrt[0]{kT} g(u - k\tilde{T}) du + \int_{j=0}^{N-1} \log \Lambda(u_j; \tilde{T})$$

To a good approximation, $\int_0^{k\tilde{T}} g(u - k\tilde{T}) du = 1$ for all k , hence

$$J(\tilde{T}) \ll n_s \tilde{K} + \int_{j=0}^{N-1} \log \left(n_s \int_{u=0}^{\tilde{K}-1} g(u_i - k\tilde{T}) + n_b \right)$$

In the last term, to a good approximation, only one pulse has a non-negligible contribution for each u_i , hence we have the further approximation

$$J(\tilde{T}) \ll n_s \tilde{K} + \int_{j=0}^{N-1} \log(n_s g([u_i]_{\tilde{T}}) + n_b) \quad (16)$$

We find the maximum of (16) numerically, using a grid search around a region of the true value. In doing so, we assume prior knowledge of the parameter domain. This is a valid assumption as the period will be known within a range bounded by uncertainties due to transmitter clock stability and Doppler predicts.

The derivative of the likelihood function is

$$\partial \Lambda(u) / \partial T = n_s \int_{u=0}^{K-1} \left(\frac{pk}{2a^2 \Gamma(1 + 1/p)} \right) \frac{u - kT}{a} \left[\exp \left(- \frac{u - kM}{a} \right) \right]^p$$

We assume that pulses are non-overlapping, hence cross terms in the numerator of (10) vanish. Similarly, the integrand vanishes away from the pulses. Hence we have

$$\text{CRB}_T \ll \left(n_s^2 \int_{u=1}^{K-1} \int_{-\infty}^{\infty} \frac{g(u) \frac{p}{a} \frac{u}{a} \left(\frac{u}{a} \right)^{p-1}}{n_s g(u) + n_b} du \right)^{-1}$$

$$= \left(\frac{(K-1)(K)(2K-1)n_s^2}{6} \int_{-\infty}^{\infty} \frac{g(u) \frac{p}{a} \frac{u}{a} \left(\frac{u}{a} \right)^{p-1}}{n_s g(u) + n_b} du \right)^{-1} \quad (17)$$

which may be evaluated numerically. In the asymptotic regions we have

$$\text{CRB}_T \ll \begin{cases} \frac{1}{n_s K^3} \frac{3a^2 \Gamma(1/p)}{p^2 \Gamma(2 - 1/p)} & n_s g(0) \in n_b \\ \frac{n_b}{n_s^2 K^3} \frac{24a^3 \Gamma^2(1/p)}{p^3 \Gamma(2 - 1/p) 2^{1/p}} & n_s g(0) \gg n_b \end{cases} \quad (18)$$

The corresponding CRB for the estimate of the frequency of the pulse train, $f = 1/(TT_s)$, in the high SNR regime is

$$\text{CRB}_f \ll \frac{1}{P_r T_i^3} \frac{hc}{\lambda} \frac{3a^2 \Gamma(1/p)}{T^2 p^2 \Gamma(2 - 1/p)}$$

For doppler estimation, the relevant error is the fractional error

$$\frac{\text{RMS}_f}{f} \ll \sqrt{\frac{1}{P_r T_i^3} \left[\frac{hc}{\lambda} \right] \frac{3(aT_s)^2 \Gamma(1/p)}{p^2 \Gamma(2 - 1/p)}} \left[\right]$$

3. COMPARISON WITH ESTIMATION FROM A COHERENTLY RECEIVED RF SIGNAL

As discussed earlier, the received RF ranging signal may be modeled as a sinusoid in additive white Gaussian noise

$$y(t) = A \cos(2\pi f_r t + \phi) + n(t)$$

where A is the signal amplitude ($A = \sqrt{2P_r}$ where P_r is the received power in the range signal), f_r is the range clock frequency, and ϕ is the phase. The additive noise $n(t)$ is Gaussian noise with power spectral density $S_n(f) = N_0/2$ Watts/Hz on $[-W, W]$ and zero elsewhere. The signal is sampled at rate $f_s = 2W$. Put $f_0 = f_r/f_s$. Estimates are based on a collection of N samples

$$y_n = A \cos(2\pi f_0 n + \phi) + w_n$$

where w_n is an IID, zero-mean, Gaussian sequence with variance $\sigma^2 = WN_0$. ML estimates and the CRBs for estimating (f_0, A, ϕ) are well known, see, e.g., Ref. 4. We simply restate the results here:

$$\begin{aligned} \text{CRB}_\phi &= \frac{2\sigma^2}{NA^2} \\ \hat{\phi}_{ML} &\ll \arctan \left(\frac{\int_{n=0}^{N-1} y_n \sin(2\pi f_0 n)}{\int_{n=0}^{N-1} y_n \cos(2\pi f_0 n)} \right) \left[\right] \\ \text{CRB}_A &= \frac{2\sigma^2}{N} \\ \hat{A}_{ML} &\ll \frac{4}{N} \int_{n=0}^{N-1} y_n \cos(2\pi f_0 n + \phi) \\ \text{CRB}_{f_0} &\ll \frac{3\sigma^2}{2A^2 \pi^2 N^3} \\ \hat{f}_{0ML} &\ll \arg \max_{f_0} \int_{n=0}^{N-1} y_n \cos(2\pi f_0 n) \end{aligned}$$

Table 1 compares the achievable RMS errors ($\text{RMS} = \sqrt{\text{MSE}} \approx \sqrt{\text{CRB}}$), or normalized versions, for ideal RF and optical links, using the high signal power asymptotes for the optical case. We see similar behavior for each parameter. The RMS phase error is inversely proportional to the product of the power and the integration time, the frequency error is inversely proportional to the product of the power and the cube of the integration time, and the intensity error goes as the power on the integration time. Hence the slopes of RMS error versus either integration time or SNR will be the same for RF and optical. In order to compare performance requires a determination of the signal and noise powers, which we treat for a sample pair of links in the next section.

3.1 Representative Link Budgets for a Mars-Earth Downlink

In this section we compare two specific candidate Mars-Earth downlinks: a Ka-band RF link with carrier frequency 32 GHz (wavelength 9.3 mm), and an optical link in the near-infrared with carrier frequency 193.5 THz (wavelength 1.55 μm). The link budgets are provided in Table 2. The Ka-band link parameters are chosen to correspond to a Ka-band Mars-Reconnaissance-Orbiter link.^{6,7} The optical link parameters are chosen to correspond to the Deep-Space-Optical Transceiver (DOT) concept.¹ The DOT concept was designed to have comparable mass and power as the Ka-band terminal. Hence the comparison is normalized for comparable burden on the

<i>parameter</i>	RMS error	
	optical	RF
$\text{RMS}_{\text{range}}(m)$	$c \sqrt{\frac{1}{T_i P_r} \left[\frac{hc}{\lambda} \right] \frac{a^2 T_s^2}{p} \left[\right]}$	$c \sqrt{\frac{1}{T_i P_r} \left[(2N_0) \right] \frac{1}{(4\pi f_r)^2} \left[\right]}$
$\frac{\text{RMS}_f}{f}$	$\sqrt{\frac{1}{T_i^3 P_r} \left[\right] \frac{hc}{\lambda} \left[\frac{3(aT_s)^2 \Gamma(1/p)}{p^2 \Gamma(2 - 1/p)} \right]}$	$\sqrt{\frac{1}{T_i^3 P_r} \left[(2N_0) \right] \frac{3}{(4\pi f_r)^2} \left[\right]}$
$\frac{\text{RMS}_{P_r}}{P_r}$	$\sqrt{\frac{1}{P_r T_i} \left[\right] \frac{hc}{\lambda} \left[\right]}$	$\sqrt{\frac{1}{P_r T_i} \left[(2N_0) \right]}$

Table 1. Comparison of achievable parameter estimation accuracies in the high SNR regime. h is Planck's constant and c the speed of light in vacuum.

spacecraft terminal. These represent current state-of-the-art candidates for a deep-space telecommunications link.

For the optical link, we assume a receive telescope diameter $D_r = 11.8$ m, corresponding to the Large Binocular Telescope in southeastern Arizona. We choose $T_s = 0.42$ ns, a target slotwidth at a range of 0.42 AU. To be conservative, we choose a worst case noise power for this link, $P_n = 3.28$ pW.¹ At long integration times, the noise is negligible, reflected in the large signal power CRBs. From these parameters, we find the received power from the link equation

$$P_r = P_t \left) \frac{\pi D_t D_r}{4R\lambda} \left[\right]^2 \eta$$

where R is the range and λ the carrier wavelength. From the link budgets we obtain

$$n_s = \frac{P_r T T_s \lambda}{hc} = 1.95 \text{ (pe/pulse)}$$

$$n_b = \frac{P_n \lambda T_s}{hc} = 0.01 \text{ (pe/slot)}$$

For the RF link, we assume a receive antenna diameter $D_r = 34$ m, corresponding to a Deep Space Network antenna. We assume a range clock modulation index of 0.8 rad, hence the received power is⁸

$$P_r = P_t \left) \frac{\pi D_t D_r f_c}{4Rc} \left[\right]^2 \eta 2J_1^2(\sqrt{2}\phi_r)$$

where J_1 is a Bessel function of the first kind or order 1. From the link equation we obtain

$$A^2 = 2P_r = 0.05 \text{ (pW)}$$

$$\sigma^2 = N_0 W = 0.002 \text{ (pW)}$$

3.2 Estimator Performance

Figures 4, 5, and 6 illustrates the ML estimator RMS error and the corresponding CRB for the operating points in Table 3. We see a threshold behavior typical of ML estimators: below a certain integration time, the estimator does no better than a random guess, above that threshold, it converges rapidly to the CRB.

Since the errors behave the same as a function of the integration time, we see the difference in the RMS errors may be factored into three constituent terms: a ratio of received powers, a ratio of noise contributions, and a ratio of the bandwidths of the signals. The ratio of the square of the received power for our presumed budgets

Ka-band Link		
f_0	carrier frequency	32.0 GHz
f_r	range clock	1.0 MHz
ϕ_r	range mod. index	0.8 rad
ϕ_c	data mod. index	0.0 rad
D_t	transmit diameter	3.0 m
D_r	receiver diameter	34.0 m
η	system efficiency	10 dB
N_o	noise spectral density	178.45 dB-mW/Hz
W	bandwidth	1.5 MHz
P_t	transmit power	35 W

Near-Infrared Link		
λ	wavelength	1.55 μm
D_t	transmit diameter	22.0 cm
D_r	receiver diameter	11.8 m
η	system efficiency	16.74 dB
α_b	noise spatial density	0.03 pW/m ²
T_s	slot width	0.42 ns
p	pulse shape	2
a	pulse width	1/2
$M = T$	PPM order	16
P_t	transmit power	4 W

Table 2. Sample Ka-band and Infrared Link Parameters

is 16 dB. This is a result of the large divergence gain when transmitting at optical wavelengths. The ratio of the noise contributions relates the shot noise of the optical signal to the thermal noise of the RF signal. As we have factored the terms, this benefits the RF signal by approximately 8 dB. The final term is the ratio of the signal features, or bandwidth, which appears as $(aT_s4\pi f_r)^2/p$ (note that for $p = 2$, the ratios of the constants is the same). For our signals, this ratio is approximately 27 dB. Hence we see gains on the order of 35 dB for range and fractional frequency estimates, and on the order of 8 dB for the power estimate, which doesn't benefit from the bandwidth gain.

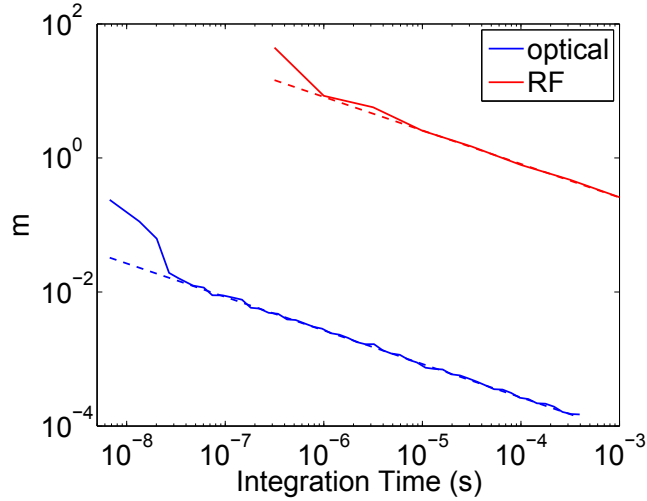


Figure 4. Achievable RMS Range Error (m) for Example RF and Optical One-Way Links. Solid line is the ML estimator performance, dashed is the CRB asymptote.

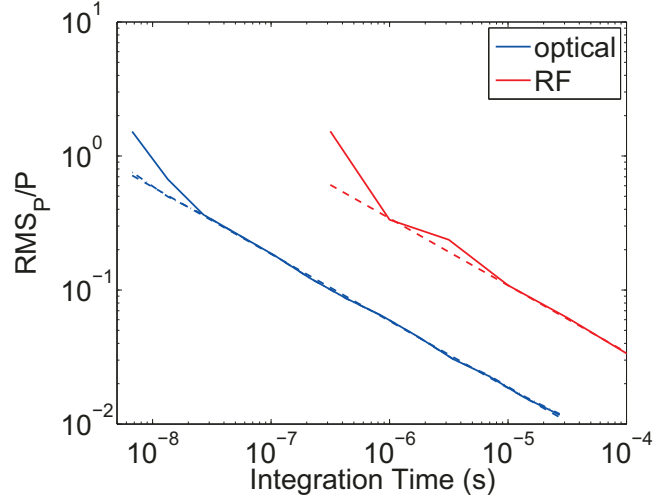


Figure 5. Achievable Fractional RMS Power Error for Example RF and Optical One-Way Links. Solid line is the ML estimator performance, dashed is the CRB asymptote, da-dot (indistinguishable from the CRB) is estimator give by (15)

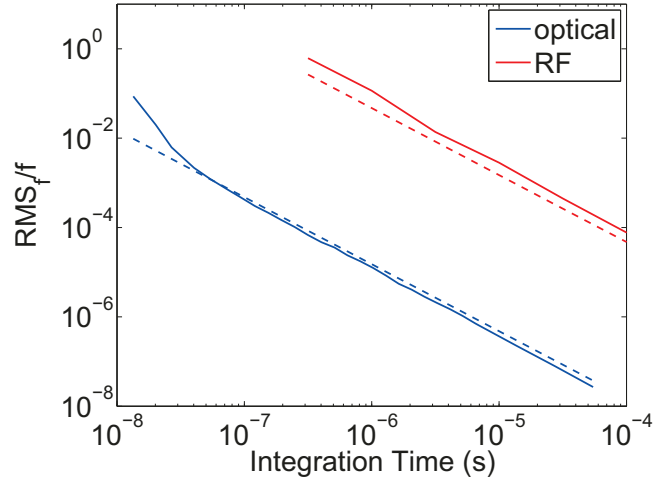


Figure 6. Achievable Fractional RMS Frequency Error for Example RF and Optical One-Way Links. Solid line is the ML estimator performance, dashed is the CRB asymptote.

4. DEGRADATIONS DUE TO DETECTOR JITTER AND CLOCK PHASE NOISE

Prior results illustrate the performance of an estimator with *ideal* subsystems. These represent bounds on the performance. Practical systems will have losses relative to the ideal. In this section we consider two non-idealities for a photon-counting receiver: detector jitter, and clock phase noise.

4.1 Detector Jitter

Suppose that we observe N photons at the output of the ideal detector over an interval S at times $\{t_1, t_2, \dots, t_N\}$. In any practical detector, photo-electrons are produced with a random offset from the time they would have been produced by an ideal detector. That is, the *observed* photo-electron arrival times are $\{t_1 + \delta_1, t_2 + \delta_2, \dots, t_i + \delta_i, \dots, t_N + \delta_N\}$, where the δ_i are random variables. We denote this additive noise process as *detector jitter*, and model the δ_i as independent of one another as well as of the arrival times $\{t_i\}$, and identically distributed with distribution

$$f_\delta(\delta) = \frac{1}{\sqrt{2\pi\sigma_\delta^2}} e^{-\delta^2/(2\sigma_\delta^2)}$$

which is a reasonably good fit to observed jitter densities,⁹ and we conjecture represents a worst-case jitter of given standard deviation. Table 3 lists the measured jitter standard deviations⁹ for an InGaAsP photo-multiplier tube (PMT) selected for high detection efficiency, a niobium nitride super-conducting single photon detector (NbN), and an InGaAsP Geiger-mode avalanche-photo-diode (APD), respectively.

Detector	σ (ns)
InGaAsP PMT	0.9154
NbN SSPD	0.02591
InGaAsP GM-APD	0.2939

Table 3. Detector Jitter for Candidate Detectors

4.2 Clock Phase Noise

In order to convert the photocurrent to photon arrival times, the photocurrent may be thresholded and used to trigger a sampling of a clock. Let

$$\begin{aligned} s(t) &= \sin \Psi(t) \\ &= \sin(2\pi f_c t + \psi(t)) \end{aligned}$$

denote the clock, where $\Psi(t)$ is the phase at time t , f_c is the nominal, or target, frequency, and $\psi(t)$ is the clock phase noise. We model the conversion of current to time by assuming the photocurrent triggers a sampling of the clock at times $t_i + \delta_i$. The sampling of the clock produces time-tags

$$T_i = \frac{\Psi(t_i + \delta_i)}{2\pi f_c} = t_i + \delta_i + x(t_i + \delta_i)$$

The phase noise term, $x(t)$, is commonly modeled as a band-limited Gaussian random process with a power-law power spectral density¹⁰

$$S_x(f) = \begin{cases} \frac{1}{(2\pi)^2} \int_{\alpha=-4}^0 h_{\alpha+2} f^\alpha & , f_j \geq f_h \\ 0 & , f_j < f_h \end{cases}$$

Numerical examples in this paper use the published phase noise specifications for the Symmetricom 9961 Hybrid Space-Qualified temperature compensated crystal oscillator (TXCO), which we consider as a candidate oscillator for a deep space communications terminal. The single-side-band (SSB) phase noise spectrum of this clock is specified in Table 4.2. We presume the clock is operated at a nominal frequency $f_c = 125\text{MHz}$, and we

frequency (Hz)	value (dBc/Hz)
10	70
10^2	105
10^3	135
10^4	150
10^5	150

Table 4. Symmetricom 9961 SSB phase noise

take the cutoff frequency to be $f_h = 2f_c$. The phase jitter contribution is dominated by the white phase noise, with phase jitter

$$\begin{aligned} \sigma_x &= \sqrt{2 \int_{10\text{Hz}}^{f_h} S_x(f) df} \\ &\ll 1 \text{ ps} \end{aligned}$$

In comparison, the smallest detector jitter contribution, for the NbN detector, is $\sigma_\delta \ll 26$ ps. Hence, for the detectors and clock we choose for our comparison, degradation due to phase noise is dominated by the detector jitter.

4.3 Performance: Mitigating Detector Jitter

Figure 7 illustrates fractional RMS frequency errors in the presence of the detector jitter and clock phase noise described above. The CRB and ML estimator for no jitter or clock phase noise (as illustrated in Fig. 6) is also shown. All cases include clock phase noise. Hence, the ‘no jitter’ curve has clock phase noise but no detector jitter, illustrating negligible loss for the specified clock phase noise. The jitter curves use the worst case of the considered detectors, the PMT, with jitter standard deviation 0.92 nsec. The curve labeled ‘no comp.’ denotes the performance when the ML estimator for no detector jitter is applied to the jittered data. We see a loss of approximately 8 dB in integration time (for the same RMS error) due to the detector jitter.

If the receiver has knowledge of the detector jitter statistics, then this information may be incorporated into the estimators. The effect of the jitter is to yield an observed arrival rate function

$$h(u) = f_{\delta} \star \Lambda(u)$$

where \star is the convolution operation. Figure 7 illustrates estimator performance with the PMT with this compensation, that is, using the proper rate function. We see a gain of approximately 3 dB from modeling and compensating for the jitter.

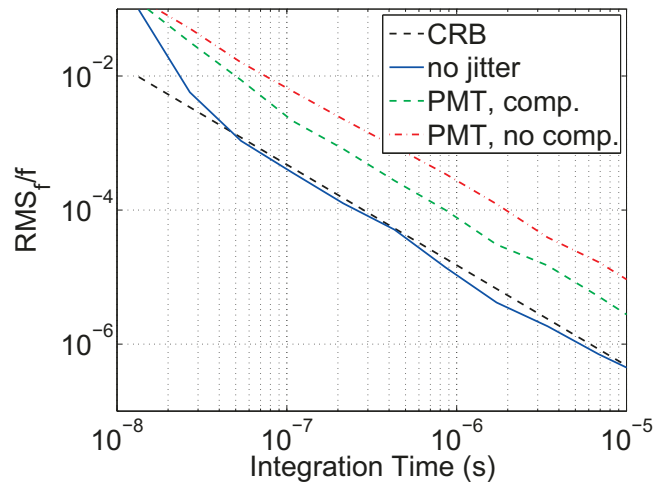


Figure 7. Performance in Detector Jitter and Clock Noise, $R = 2.0$ AU

5. CONCLUSIONS/DISCUSSION

APPENDIX A. CRAMER RAO BOUND

Here we derive an expression for the CRB of parameters of the intensity function of a Poisson process. Let $\Lambda(u)$ be the intensity function of a Poisson process, $\lfloor (u)$ the (random) counting process induced by $\Lambda(u)$, and $i(t) = d\lfloor (u)/du$ —in our case, the resulting normalized photo-current (a sum of discrete photo-electrons). Note that

$$E(i(u)) = \Lambda(u)$$

Let $\{u_i\}_{i=0, \dots, N-1}$ be the collection of arrival times over an observation interval T_i , and θ an unknown parameter characterizing $\Lambda(u)$. We have

$$\frac{\partial}{\partial \theta} \log p(\{u_i\}, N; \theta) = \int_{T_i} \dot{\Lambda}(u) du + \sum_{i=0}^{N-1} \frac{\dot{\Lambda}(u_i)}{\Lambda(u_i)} \quad (19)$$

where $\dot{\Lambda}(u) = \frac{\partial}{\partial u} \Lambda(u)$. Let $h(u)$ be some deterministic function of u . Note that

$$\int_i h(u_i) = \sqrt{i(u)} h(u) du$$

$$E \left[\int_i h(u_i) \right] = \sqrt{\Lambda(u)} h(u) du$$

Applying this to (19) we have

$$E \left[\frac{\partial}{\partial \theta} \log p(\{u_i\}, N; \theta) \right] = \sqrt{\frac{1}{T_i}} \left(\ddot{\Lambda}(u) \Lambda(u) + \frac{\dot{\Lambda}^2(u_i)}{\Lambda(u_i)} du \right)$$

$$= \sqrt{\frac{1}{T_i}} \frac{\dot{\Lambda}^2(u)}{\Lambda(u)} du$$

ACKNOWLEDGMENTS

Many thanks to Charles Greenhall, JPL, for discussions on clock noise and for providing software clock noise generators.

REFERENCES

- [1] Biswas, A., Hemmati, H., Piazzolla, S., Moision, B., Birnbaum, K., and Quirk, K., “Deep-space optical terminals (DOT) systems engineering,” *IPN Progress Report* **42–183** (November 2010).
- [2] Yuen, J. H., ed., [*Deep Space Telecommunications Engineering*], ch. Receiver Design and Performance Characteristics, Plenum Press, New York (1983).
- [3] Snyder, D. L., [*Random Point Processes*], Wiley (1975).
- [4] Kay, S. M., [*Fundamentals of Statistical Signal Processing: Estimation Theory*], Prentice Hall (1993).
- [5] Erkmén, B. I. and Moision, B., “Maximum likelihood time-of-arrival estimation of optical pulses via photon-counting photodetectors,” in [*Proceedings of IEEE International Symposium on Information Theory*], 1909–1913, IEEE (June 2009).
- [6] Williams, W. D., Collins, M., Hodges, R., Orr, R. S., Sands, O. S., Schuchman, L., and Vyas, H., “High-capacity communications from Martian distances,” Tech. Rep. 2007-214415, NASA/TM (December 2007). available at <http://gltrs.grc.nasa.gov>.
- [7] Shambayati, S., Morobito, D., Broder, J. S., Davarian, F., Lee, D., Mendoza, R., Britcliffe, M., and Weinreb, S., “Mars Reconnaissance Orbiter Ka-band (32 GHz) demonstration: Cruise phase operations,”
- [8] Kinman, P. W. and Berner, J. B., “Two-way ranging during early mission phase,” *Proceedings of the IEEE Aerospace Conference* (March 2003).
- [9] Moision, B. and Farr, W., “Communication limits due to photon detector jitter,” *IEEE Photonics Technology Letters* **20**, 715–717 (May 2008).
- [10] Rutman, J. and Walls, F. L., “Characterization of frequency stability in precision frequency sources,” *Proceedings of the IEEE* **79** (June 1991).